Conversion of short optical pulses to terahertz radiation in a nonlinear medium: Experiment and theory

N. N. Zinov'ev*
Department of Physics, University of Durham, Durham DH1 3LE, United Kingdom
and A. F. Ioffe Physical Technical Institute, 194021 St. Petersburg, Russia

A. S. Nikoghosyan
Department of Microwave Engineering, Yerevan State University, Yerevan 375025, Armenia

R. A. Dudley
National Physical Laboratory, Teddington, Middlesex TW11 0LW, United Kingdom

J. M. Chamberlain
Department of Physics, University of Durham, Durham DH1 3LE, United Kingdom
(Received 20 April 2007; revised manuscript received 19 July 2007; published 13 December 2007)

We report on the frequency and time domain analysis of electromagnetic terahertz radiation generated by nonlinear conversion of short optical pulses crossing boundaries of nonlinear material. Analysis and comparison with experiment have unequivocally established that the nature of collinear radiation at terahertz frequencies relates to the phenomenon of transition radiation produced by the instantaneous creation (at the input interface) and extinction (at the output interface) of the moving polarization charge formed by the nonlinear coupling of the pump electromagnetic fields. The mechanism is analogous to the phenomena of transition radiation of moving free charges, in particular, to the radiation mechanism discussed in the Tamm problem.

DOI: 10.1103/PhysRevB.76.235114 PACS number(s): 42.65.Ky, 41.60.−m, 78.47.+p

I. INTRODUCTION

In spite of remarkable achievements in nonlinear optics, there remains a fundamental issue, related to the mechanism of nonlinear wave conversion (NLWC) of a short optical pulse into difference and sum frequency radiation, that does not yet seem to have a clear interpretation.

According to the fundamentals of nonlinear optics,[1,2] difference frequency generation (DFG), being a phenomenon of a coherent nonlinear three-wave interaction, enables the nonlinear conversion of pump electromagnetic (EM) waves into electromagnetic radiation (EMR) at a frequency that can be the difference combinations of the pump wave frequencies including zero frequency, optical rectification (OR).[1–3] The spectrum of a short pulse contains a broad band of frequencies around a carrier frequency ω_0.[4,5] Nonlinear conversion of such pulse in a medium generates EMR at various frequency combinations: DFG/OR, sum frequency generation (SFG), and second harmonic generation (SHG). According to NLWC theory,[2,6] originally developed for interactions of continuous plane harmonic waves, coherent conversion on the microscopic scale is interpreted as the result of constructive interference of two partial waves, the inhomogeneous wave (IHW) and the homogeneous wave (HW). These waves are related to the mathematical constructions of the same name which provide the solution of the nonlinear wave equation.[2] When extrapolated to the case of the interaction of wave packets, the NLWC model should deal with the interaction of two wave packets, HW and IHW. For DFG, HW should be the bunch of waves in a nonlinear medium around the conversion frequencies ω with wave vectors $k_\omega = \omega/c(\omega)$. IHW is the wave packet with the same frequencies $\omega=\Delta\omega_p$, but with the wave vectors $k_{\omega_p}-k_{\omega_p+\Delta\omega_p}\sim\omega/v_g(\omega_p)$. Here, $c(\omega)$ and $v_g(\omega_p)$ are the phase velocities of the converted terahertz wave and the group velocity of the IHW (equal to the pump wave) packet and $\Delta\omega_p$ is the bandwidth of the pump. It is believed that a microscopic effect of NLWC is due to the constructive interference of IHW and HW[2,6] if the phase matching conditions (PMCs) are met. PMCs come from the conservation laws of wave vector and energy and reduce to a simple equality between the velocities of interacting waves, namely, $c(\omega)=v_g(\omega_p)$. In practice, however, because of velocity dispersion, these PMCs are rarely met in full, at least for a broad band of frequencies. Then, the constructive interference of IHW and HW occurs on the scale of the coherence length L_{coh}. This commonly accepted approach[1–10] assumes that both the HW and IHW begin constructively to interfere and build up the nonlinear effect microscopically within L_{coh} from the input interface. They further "walk off" and, therefore, do not contribute to the nonlinear conversion on the scale $z>L_{coh}$. The interference of HW and IHW explains the Maker fringes,[8,9] one of the experiments forming the cornerstone of nonlinear optics. So far, a considerable number of papers published on nonlinear interactions of wave packets have used the NLWC model outlined above to interpret their results, e.g., Refs. 5 and 11–18. Some of these works considered the problem using a CW plane wave approach;[2,12,17,18] the others used a method based on the d'Alembert symbolic approach to the wave equation,[13] or considered the particular case of exact phase matching.[11,15,16]

The NLWC model was not called into question until the publication of Ref. 19, where a new property of DFG was reported: twinning of pulses of terahertz EMR generated

with short optical pump pulses in an electro-optic crystal. The time delay between the twins was equal to the difference of propagation times for terahertz and pump pulses. From this, evidence[19] tentatively attributed the twin pulses of terahertz EMR to EM radiation emanating from boundaries. However, the twin pulse structure could alternatively be explained within the NLWC model[2] as the signature of a three-wave interaction in the time domain by associating the pair of pulses with the HW and IHW, respectively. Indeed, according to Refs. 1 and 2, the HW and IHW pulses are generated simultaneously in the same volume of sample adjacent to the input interface boundary. Because of dispersion, the HW and IHW walk off with different velocities, c and v_g, respectively. Thus, the difference in the arrival time of the HW and IHW pulses at the end of sample of length L would be given by $\Delta t = L/c - L/v_g$. This value of Δt is exactly equal to the time split measured in Ref. 19. A brief outline of NLWC model applied to DFG is given in the Appendix.

An alternative to the NLWC model approach to the generation of EMR with short optical pulses has been proposed phenomenologically in 1962 (Ref. 20) by drawing analogies between the generation of EMR from EMR and the radiation phenomena of moving charges.[21–28] An intense optical pulse in a nonlinear material is accompanied by a cloud of space polarization charge with the density $\rho_d = -\nabla \mathbf{P}^{NL}$, where $\mathbf{P}^{NL} = \hat{\chi}^{(2)} : \mathbf{E}_p \mathbf{E}_p^{\star}$, $\hat{\chi}^{(2)}$ is the nonlinear susceptibility tensor of the second rank and $\mathbf{E}_p$ is the electric component of the incident pump electric field. The propagation of this polarization charge, according to the proposition of Ref. 20, could be the source of the EMR. In Ref. 20, two mechanisms for the generation of such EMR were suggested. One was the noncollinear mechanism of EMR analogous to the Vavilov-Cherenkov effect.[27,28] For DFG, the low frequency dielectric constant $\epsilon(\omega)$ normally exceeds the value of the dielectric constant at pump carrier frequencies $\epsilon(\omega_0)$ because of the contribution to $\epsilon(\omega)$ from phonons: $\epsilon(\omega) > \epsilon(\omega_0)$. A similar kind of inequality holds for SHG in a semiconductor, if the pump frequency ω_0 is at the mid gap position $\hbar\omega_0 \pm \Delta\omega \lesssim E_g/2$ and $2(\omega_0 \pm \Delta\omega) \lesssim E_g$, where E_g is the forbidden gap. Under such conditions, the resonance enhancement factor $(\hbar 2\omega_0 - E_g)^{-1}$ increases the value of $\epsilon(2\omega_0)$. In both cases, the velocity v_g of the pump pulse bearing the polarization charge becomes greater than the phase velocity of the converted EMR, creating the conditions for the Vavilov-Cherenkov generation of EMR. For a single pulse and DFG type of nonlinear wave conversion, the conservation laws for wave vector and energy, $\Delta\mathbf{k}_0 = \mathbf{k}$ and $\Delta\omega_0(\mathbf{k}_0) = \Delta\omega(\mathbf{k})$, lead to the PMC of a noncollinear type:

$$\omega \equiv \Delta\omega \approx \frac{\partial\omega}{\partial\mathbf{k}_0} \cdot \mathbf{k} = v_g \cdot k \cos\theta, \tag{1}$$

where $v_g = |\partial\omega/\partial\mathbf{k}_0|$ is the group velocity of the pump at frequency ω_0 and k is the wave vector of the converted wave radiated at angle θ. The angle θ obeys the relationship $\cos\theta = c/v_g$, where $\omega/k = c$ is the phase velocity of the converted wave. For a broadband DFG at terahertz frequencies, the maximum value of θ normally reaches 30°–70° for typical crystals such as ZnTe, GaAs, $LiNbO_3$, etc. Although Eq. (1) seems to establish PMC, several complications remain. Firstly, Eq. (1) is subject to dispersion, $\theta \equiv \theta(\omega, \omega_0)$, and, therefore, the angle θ varies over a large scale. Secondly, Eq. (1) is the relationship between the longitudinal projections of wave vectors; it is not a complete PMC. The deficit of the transverse wave vector for a single pump pulse is derived from the uncertainties of pump pulse localization, e.g., if the pump beam is tightly focused. Thirdly, even in the most favorable case of weak dispersion, condition (1) leads to noncollinear EMR at the angle θ that normally exceeds the angle of total internal reflection. This blocks efficient coupling of this type of EMR into free space. The Vavilov-Cherenkov type of terahertz DFG so far has been identified[20,29,30] and detected in the same crystal[31–33] by mapping the Cherenkov cone formed by converted field, but it encounters serious problems of coupling into free space.[34,35]

According to another proposition of Ref. 20, a high frequency collinear EMR could begin with a pulse crossing the boundary between a linear and nonlinear medium or two media, one of which has a greater nonlinearity than the other. When an optical pulse traverses the interface between linear and nonlinear media, a net space polarization charge is created in the nonlinear medium, and instantaneously accelerated to the optical pulse velocity. When the optical pulse leaves the nonlinear medium, the polarization charge instantaneously disappears, which is equivalent to the charge stopping. Between these two radiation events, the polarization charge moves uniformly with the velocity of the optical pulse. At this stage, i.e., in the bulk, the charge can radiate only if the conditions for the Vavilov-Cherenkov effect are met. This model scenario is very similar to the radiation events of the start-stop motion of a charged particle in homogeneous media, which has been considered earlier by Tamm.[21] This radiation problem is named as the "Tamm problem" and has received attention in many subsequent papers (see, e.g., Ref. 22 and references cited therein). If the mechanism of EMR during nonlinear wave conversion (resembling the Tamm problem case) does indeed exist, it can be related to the wide class of transition radiation (TR) phenomena obtained in high energy particle physics when moving charges cross boundaries between two different media[23–25] and which have been confirmed experimentally in many papers (e.g., see Refs. 36–38). However, unlike radiation phenomena with moving charges,[25] nonlinear coupling between the pump fields is the essential condition for creation of polarization charge. Therefore, such a radiation mechanism with optical pulses can only be observed in a nonlinear medium. TR EMR could be generated in a collinear geometry and, unlike Vavilov-Cherenkov EMR, TR does not require any specific relation between the velocities. The strength of TR with moving charges is proportional to the formation length,[26] i.e., the length over which radiation from a moving source is established. It corresponds to a definition of coherence length. Then, TR with short optical pulses should be emitted from the regions on the scale of the formation length which are adjacent to the input and output boundaries. It is clear that within this model, the time split between the pulses emitted from input and output surfaces of a nonlinear medium is $\Delta t = L/c - L/v_g$, where c and v_g are the averaged velocities over the emission bandwidth and L is the thickness of nonlinear medium.

Thus, the brief review given above shows that understanding of NLWC phenomena is still far from complete. The existing ambiguity (primarily associated with the mechanism of nonlinear wave generation, localization of the generation regions, and the time- and frequency-domain kinetics of nonlinear wave generation) demands a reappraisal of the theoretical foundations of EMR with short optical pulses in nonlinear media, together with comprehensive time domain experimental research into the coherent generation of EMR pulses. A brief report on our research, proving both theoretically and experimentally the mechanism of terahertz TR generation, has been published recently in Ref. 39. In this paper, we extend the theory considering two model cases of infinite and semi-infinite nonlinear media, extending them into the practically important case of terahertz generation under arbitrary wave vector mismatch (WVM) conditions in a nonlinear slab placed in a linear medium. To compare with experimentally measured signals, we derive the analytical dependencies for DFG terahertz wave forms emitted into the remote free space zone in both forward and backward geometries. We present experimental results for two nonlinear samples, one with WVM $\Delta k \neq 0$ ($LiNbO_3$) and the other with WVM $\Delta k \rightarrow 0$ (ZnTe). We also compare the obtained data with the predictions of existing NLWC model.

This paper is organized as follows. Section II considers nonlinear conversion of optical pulses into terahertz EMR at arbitrary WVM in infinite and semi-infinite nonlinear media and a nonlinear slab. It closely examines the collinear conversion process, terahertz pulse structure, and the dependence of their temporal and spectral kinetics on slab thickness, WVM conditions, dispersion, and absorption in the slab. Section III is devoted to experimental procedures and discussion. The Appendix briefly outlines the theoretical scheme of NLWC model and compares the predictions of existing NLWC model with the experimental time domain data and results of our theory. Section IV contains a summary and conclusion.

II. THEORY

We start from the time-frequency domain calculations of terahertz EMR resulting from the conversion of short optical pump pulse traversing a nonlinear material. We calculate collinearly and anticollinearly propagating EM fields in infinite and semi-infinite nonlinear media and the wave forms of THz emission radiated in collinear, forward and anticollinear, backward directions from a nonlinear slab held in air under the condition of arbitrary value of WVM $\Delta k \neq 0$. The solutions for terahertz wave forms, thus obtained, are compared with the experimental data in Sec. III.

A. Coherent generation of electromagnetic radiation in a nonlinear medium

To investigate time domain and spectral kinetics of terahertz EMR generated with short optical pulses theoretically, we consider the process of nonlinear wave packet conversion, a dynamic analog of OR/DFG, inside a nonlinear dielectric medium. The solution of the problem begins from the set of two equations,[40,41] the wave equation,

$$\nabla^2 \mathbf{E}_i(\mathbf{r},t) - \frac{1}{c_0^2}\int_{-\infty}^{+\infty} dt' \epsilon(t-t')\frac{\partial^2}{\partial t'^2}\mathbf{E}_i(\mathbf{r},t') = \mu_0 \int_{-\infty}^{+\infty} dt' \sigma(t-t')\mathbf{E}_i(\mathbf{r},t') + \mu_0 \frac{\partial^2 \mathbf{P}^{NL}(\mathbf{r},t)}{\partial t^2} + \nabla \cdot (\nabla \cdot \mathbf{E}_i(\mathbf{r},t)), \quad (2)$$

and the Poisson's equation,

$$\epsilon_0 \int_{-\infty}^{+\infty} dt' \epsilon(t-t') \nabla \cdot \mathbf{E}(\mathbf{r},t') = -\nabla \cdot \mathbf{P}^{NL}(\mathbf{r},t). \quad (3)$$

For a single pulse, nonlinear polarization is given by

$$\mathbf{P}^{NL}(\mathbf{r},t) = \epsilon_0 \int_{-\infty}^{+\infty} dt' \chi^{(2)}(t-t')\mathbf{E}(\mathbf{r},t')\mathbf{E}(\mathbf{r},t') + \cdots . \quad (4)$$

For the sake of generality, we include in Eqs. (2) and (3) the term describing the loss for converted field $\mathbf{E}_i(\mathbf{r},t)$ due to finite conductivity by free carriers $\sigma(\omega)$. In nonlinear dielectrics and wide band gap materials (no two-photon absorption), free carrier conductivity is insignificant. Therefore, in the further treatment, we omit this term. In Eqs. (2) and (3), we assume a case of weak nonlinearity, i.e., there is no depletion of energy from the pump wave, and also neglecting the pump pulse distortion. The form of expressions (2)–(4) assumes that nonlocal effects and spatial dispersion are neglected leaving only the effects of time and/or frequency dispersion.

We note that Eqs. (2) and (3) describe radiation phenomena of a moving polarization charge with density $\rho_d = -\nabla \cdot \mathbf{P}^{NL}$. The second term in the right-hand side (rhs) of Eq. (2) is known as the time derivative of the nonlinear term of displacement current $\mathbf{J}_d^{NL}$. Then, the expression for $\mathbf{J}_d^{NL}$ can be expressed in the "hydrodynamic" form as the flux of polarization charge,

$$\mathbf{J}_d^{NL}(\mathbf{r},t) = \partial \mathbf{P}^{NL}(\mathbf{r},t)/\partial t = \nabla \cdot \mathbf{P}^{NL}(\mathbf{r},t) \cdot \partial \mathbf{r}/\partial t = -\rho_d(\mathbf{r},t)\mathbf{v}. \quad (5)$$

This provides formal justification of the correctness of the preceding statement. Here, $\mathbf{v}$ is the velocity of polarization charge. It is known that, unlike conduction charge, the polarization charge is a bound charge. In fact, this distinction is strictly limited to the static case and becomes meaningless for high frequency time dependent fields. With a propagating wave packet, the envelope moves with the group velocity, so also does the polarization charge induced due to nonlinear coupling of the pump fields. When formulated in this way, Eqs. (2) and (3) resemble the familiar set of equations from the theory of radiative phenomena of moving charges.[25] The only difference is that, instead of an external moving charge, in this case, the polarization charge is formed in the medium due to the nonlinear relationship between fields; it subsequently moves uniformly further through the medium. The wave equations [Eq. (2)] and the Poisson's equation [Eq. (3)] describe both collinear-anticollinear and noncollinear radia-

tion phenomena accompanying the propagation of this polarization charge.

As stated in Sec. I, the output radiation coupling of noncollinear EMR is greatly restricted into free space in the forward direction. For this reason, we restrict ourselves to the collinear nonlinear process of nonlinear conversion. This takes into account only the terms from the source's expansion in plane waves with zero wave vector angular components. Therefore, for collinear and anticollinear interactions, we may retain only the dependence of the converted field on the z coordinate because of axial symmetry along the z axis. This approximation is relevant to the cases of one-dimensional geometry or with moderate focusing of the pump beam when the confocal parameter of the focusing optics is much bigger than the medium thickness. Under this condition, the wave front of pump field within the medium volume can be considered as nearly plane but is restricted to the cross section square of the pump beam. Taking into account the tensor relationship between the terahertz field and the linear polarization, both the field $\mathbf{E}(\mathbf{r},t) \equiv \mathbf{E}(z,t)$ and polarizations $\mathbf{P}^{NL}(\mathbf{r},t) \equiv \mathbf{P}^{NL}(z,t)$ can have, in general, both longitudinal and transverse components. Accordingly, we separate electric field and polarization vectors into longitudinal and transverse components using the following expressions:

$$\mathbf{E}(z,t) = \mathbf{z}_0 E_{\parallel}(z,t) + \mathbf{E}_{\perp}(z,t), \tag{6}$$

$$\mathbf{P}^{NL}(z,t) = \mathbf{z}_0 P_{\parallel}^{NL}(z,t) + \mathbf{P}_{\perp}^{NL}(z,t), \tag{7}$$

where $\mathbf{z}_0$ is the unit vector in the direction of the z axis. The index "$\perp$" labels the polarization state in the plane X-Y, i.e., $\perp$ refers to the polarization along either the X or Y axis, or to a combination of X and Y. After substitution of Eqs. (6) and (7) into Eqs. (2) and (3), and grouping similar polarization components, we obtain two equations for $E_{\parallel}(z,t)$ and $\mathbf{E}_{\perp}(z,t)$:

$$-\frac{\partial^2 \mathbf{E}_{\perp}(z,t)}{\partial z^2} + \frac{1}{c_0^2}\int_{-\infty}^{+\infty} dt' \epsilon(t-t') \frac{\partial^2}{\partial t'^2}\mathbf{E}_{\perp}(z,t') = -\mu_0 \frac{\partial^2 \mathbf{P}_{\perp}^{NL}(z,t)}{\partial t^2}, \tag{8}$$

$$\frac{1}{c_0^2}\int_{-\infty}^{+\infty} dt' \epsilon(t-t') \frac{\partial^2}{\partial t'^2} E_{\parallel}(z,t') = -\mu_0 \frac{\partial^2}{\partial t^2} P_{\parallel}^{NL}(z,t). \tag{9}$$

The second equation of this set, Eq. (9), is simply the operator relationship between $E_{\parallel}(z,t)$ and $P_{\parallel}^{NL}(z,t)$. Therefore, without loss of generality, we can choose the geometry with zero components of the nonlinear susceptibility tensor $\hat{\chi}^{(2)}$ responsible for the $P_{\parallel}^{NL}(z,t)$ and neglect the transverse beam confinement effect. Finally, we obtain the single wave equation for the terahertz electric field $\mathbf{E}_{\perp}(z,t)$ in the form of Eq. (8). We represent a pump optical pulse in the rhs of Eq. (8) as the product of the Gaussian pulse envelope and the plane carrier wave at the frequency ω_p:

$$\mathbf{E}_p(z,t) = \frac{1}{2}\mathbf{e}_{\perp} E_0 \exp\left[-\frac{\left(t-\frac{z}{v_g}\right)^2}{4\tau_p^2}\right] \exp\{i[\omega_p t - k(\omega_p)z]\} + \text{c.c.}, \tag{10}$$

where v_g is the group velocity of the pump wave packet, the pump pulse, $v_g = c_0[n(\omega_p) + \omega_p dn(\omega_p)/d\omega_p]^{-1}$, and τ_p is a parameter related to full width at half maximum.[5,42] The scalar component $E_{\perp}(z,\omega)$ of the terahertz field (to be used in the calculations below) is $E_{\perp}(z,\omega) = \mathbf{e}_{\perp} \cdot \mathbf{E}_{\perp}(z,\omega)$, where $\mathbf{e}_{\perp}$ is the polarization vector in the plane perpendicular to the beam axis. To contract the formulas, we use the relationship $\hat{\chi}^{(2)} = \Sigma_{i,j=k} \mathbf{e}_{\perp i} \hat{\chi}_{ijk}^{(2)} \mathbf{e}_{\perp j} \mathbf{e}_{\perp k}$. For definiteness, we choose the polarization of $E_{\perp}(z,\omega) = E_x(z,\omega)$. Then, with the use of Eq. (10), the scalar form of the nonlinear wave equation describing the collinear process of terahertz generation is transformed into the form

$$-\frac{\partial^2 E_x(z,t)}{\partial z^2} + \frac{1}{c_0^2}\frac{\partial^2}{\partial t^2}\int_{-\infty}^{+\infty} dt' \epsilon(t-t') E_x(z,t') = -\frac{1}{c_0^2}\frac{\partial^2}{\partial t^2}\int_{-\infty}^{+\infty} dt'' \hat{\chi}^{(2)}(t-t'') E_0^2 \exp\left[-\frac{(t''-z/v_g)^2}{2\tau_p^2}\right]. \tag{11}$$

In Eq. (11), we leave the source term in the form describing DFG/OR processes. Consideration of SHG/SFG processes can be conducted in similar way. The solution of Eq. (11) describes the field generated in a nonlinear medium from moving source represented by rhs. For the sake of generality, we consider below the generation of terahertz field in infinite and bounded media.

B. Infinite nonlinear medium

We first turn to a model problem of an infinite nonlinear medium lossless for the radiation of the pump pulse. This case allows us to draw up the major conclusion on the location of EMR generation from nonlinearly coupled pump EM fields. To obtain the solution of the wave equation [Eq. (11)], we apply the Fourier transform to Eq. (11) for the pair of conjugated variables $t \to \omega$. With the notation $S(\omega) = (\omega^2/c_0^2)\sqrt{2\pi}\hat{\chi}^{(2)} E_0^2 \tau_p \exp(-\omega^2\tau_p^2/2)$ and $c = c_0/\sqrt{\epsilon(\omega)} = c_0/n(\omega)$, Eq. (11) has the form of the inhomogeneous Helmholtz equation:

$$\frac{d^2 E_{\perp}(z,\omega)}{dz^2} + \frac{\omega^2}{c^2} E_{\perp}(z,\omega) = -S(\omega)\exp\left(i\frac{\omega}{v_g}z\right). \tag{12}$$

The solution of Eq. (12) is given as the convolution integral of the Green's function with the rhs:

$$E_x(z,\omega) = S(\omega)\int_{-\infty}^{+\infty} d\xi G(z,\xi)\exp\left(i\frac{\omega}{v_g}\xi\right). \tag{13}$$

The Green's function $G(z,\xi)$ is found from the solution of

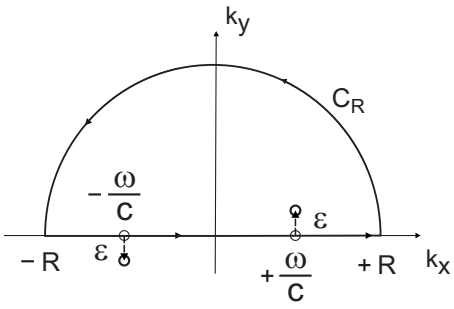

FIG. 1. Contour of integration C_R used to calculate Eq. (15).

$$\frac{d^2G(z,\xi)}{dz^2} + \frac{\omega^2}{c^2}G(z,\xi) = \delta(z-\xi). \tag{14}$$

Equation (14) is solved using Fourier transform $z \to k$ on Eq. (14). Then, the solution $G(z,\xi)$ is given as

$$G(z,\xi) = -\frac{1}{2\pi}\int_{-\infty}^{+\infty} dk \frac{e^{ik(z-\xi)}}{k^2 - \left(\frac{\omega}{c}\right)^2}. \tag{15}$$

The integration of Eq. (15) is performed applying the residue theorem to the contour C_R shown in Fig. 1, where the poles ω/c were added with an infinitesimal imaginary part $\epsilon \to 0$. As consequence, the Green's function $G(z,\xi)$ is obtained in the form

$$G(z,\xi) = -\frac{i}{2\left(\frac{\omega}{c}\right)} \exp\left[i\frac{\omega}{c}(z-\xi)\right]. \tag{16}$$

It obeys the boundary conditions at infinity, which are Sommerfeld radiation conditions.[43–45] Then, using Eq. (13), terahertz field generated in the bulk of infinite nonlinear medium in collinear direction is given by

$$E_x(z,\omega) = i\pi c\frac{S(\omega)}{\omega}\exp\left(i\frac{\omega}{c}z\right)\int_{-\infty}^{+\infty}\frac{\exp\left[-i\left(\frac{1}{c}-\frac{1}{v_g}\right)\omega\xi\right]}{2\pi}d\xi. \tag{17}$$

The integral in rhs of Eq. (17) represents δ function of the argument $\omega(1/c-1/v_g)$, that is, the WVM quantity. This leads to the conclusion that there is no nonvanishing radiation contribution everywhere in the bulk of nonlinear medium in the collinear direction, $k \| z$, if and only if there is a WVM, namely, $1/c \neq 1/v_g$, no matter what the strength of this inequality is. In fact, this is an expected result that finds a close analogy in the theory of transition radiation phenomena of uniformly moving charges.[23,25,26] It is simply the mathematical form of the well known physical principle adopted to the case of interacting EM waves that uniformly moving charge in a homogeneous medium does not radiate, unless condition (1) for the Vavilov-Cherenkov (VC) EMR is fulfilled. For collinear radiation, $\theta=0$ and Eq. (17) requires the exact match of c and v_g. The marked behavior of Eq. (17) means that the physics of EMR generation at nonlinear wave interaction is more complex than a trivial nonlinear mixing of EM waves. In practice, it is quite impossible to observe the exact condition $1/c=1/v_g$ due to dispersion. In the strict sense, this condition can only be met for a single frequency rather than for a frequency band. Therefore, the EMR field generated in the collinear direction at nonlinear coupling of EM fields should be treated as the radiation phenomenon entirely related to the interface boundaries. The field is emitted from the boundary of two media with different nonlinear dielectric constants (linear-nonlinear media, two different nonlinear media), crossed by optical pulse. In the bulk of the medium, however, collinear radiation can only occur if and only if $v_g=c$, that is, the exact equivalent of vanishing WVM, $\Delta k \to 0$. To prove this assertion, we further consider the cases of a semi-infinite medium and a nonlinear slab related to nonlinear optic experiments.

C. Bounded nonlinear media

In a bounded medium, the solution of the wave equation with the form of the source term [Eq. (11)] sums up multiple reflections of the terahertz EMR that have been converted from the first transit flight of the pump pulse; these provide the meaningful part of the solution and contain information on the physical processes of nonlinear generation of terahertz EMR. The form of Eq. (11) does not include the contributions to terahertz EMR from the multiple reflections of the pump pulse inside the slab, which is an equivalent to the assumption of a sample being antireflection coated to avoid multiple reflection of the pump pulse. Bearing in mind the quadratic dependence of the source term on the pump field in the rhs of Eq. (11), we assume that the contribution to the terahertz wave form from the multiple reflections of the pump pulse inside the slab is negligibly small.

The general solution of Eq. (12) is the sum of the solution of the homogeneous equation and the particular solution of the inhomogeneous equation [Eq. (12)]. The physical meaning of the rhs of Eq. (12) is the Fourier transform of the time derivative of the nonlinear term of displacement current that has been created by the moving polarization charge, i.e., a moving source, with velocity v_g [Eq. (5)]. The difference between Eq. (12) and the equations from the theory of TR of moving charges[25] is in the rhs source term. In the theory of radiation phenomena of moving charges, the polarization of the source current and current direction are parallel to each other. Unlike this, in Eq. (12), the direction of source electric field lies in the transverse plane, but the source moves along the z axis. Another difference is in the nature of moving charge. Instead of uniformly moving external charges, in this case, a polarization charge is formed due to nonlinear coupling of EM pump fields. The important spatial parameter, the formation length, defines the amplitude of the emission process[26] during wave conversion. The formation length is defined in several equivalent ways, namely, as the length where the radiation from a source is established, as the length where the radiation field is separated from the field of charge, or as the length from which all waves are radiated with phases less than π. Assuming a source radiating EMR $E(r,t)=E_0\exp(i\mathbf{kr}-i\omega t)$ at an angle θ and propagating with

the velocity of v_g, the phase difference of EMR, $\Delta\phi$, between two arbitrary points of the source trajectory separated by distance R is given by $\Delta\phi=\omega r/v_g-\mathbf{k}\cdot\mathbf{r}$. Then, using the definition of the formation or coherence length given above, it takes the form

$$L_{coh}^{BW/FW}(\theta,\omega)=\frac{\pi}{\frac{\omega}{v_g}\left|\left(1\pm\frac{v_g}{c}\cos\theta\right)\right|}, \tag{18}$$

where the signs "−" and "+" in the denominator correspond to the EMR emitted into the forward (FW) and backward (BW) hemispheres $\{-\pi/2,\pi/2\}$, respectively. For collinear and anticollinear geometries, we let $\theta=0$ and $L_{coh}^{BW/FW}(\omega)=L_{coh}^{BW/FW}(\theta=0,\omega)$.

1. Semi-infinite nonlinear medium

The existence of an interface boundary in this case introduces an important difference in the treatment of the nonlinear radiation problem. The boundary condition (BC) for **E** and **H** fields requires the continuity of the tangential components of the electric and magnetic fields at the interfaces $z=0$ (input boundary of semi-infinite medium). The BC matches the electric component in free space with the total electric field inside the medium at $z=0$. Then, the collinear field inside a semi-infinite nonlinear medium is

$$E_x(z,\omega)=C_1\exp\left(i\frac{\omega}{c}z\right)+\frac{L_{coh}^{FW}L_{coh}^{BW}S(\omega)}{\pi^2}\exp\left(i\frac{\omega}{v_g}z\right). \tag{19}$$

The expression for electric field outgoing into free space from the boundary at $z=0-$ is the solution of homogeneous wave equation

$$\frac{d^2E_x(z,\omega)}{dz^2}+\frac{\omega^2}{c_0^2}E_x(z,\omega)=0. \tag{20}$$

This describes the terahertz field $E_\perp(z,\omega)$ backward irradiated into the left-hand half of free space at $z<0$,

$$E_x(z,\omega)=C_{BW}\exp\left(-i\frac{\omega}{c_0}z\right). \tag{21}$$

For the chosen geometry (normal incidence, polarization of **E** vector along the x axis, polarization of **H** vector along the y axis, and the z axis is the propagation axis), the relationship between the electric and magnetic components takes the form

$$-\frac{i}{\mu_0\omega}\frac{dE_x(z,\omega)}{dz}=H_y(z,\omega). \tag{22}$$

Then, the BCs for $E_x(z,\omega)$ and $H_y(z,\omega)$ at $z=0$ interface are given by

$$E_x(z=-0,\omega)=E_x(z=+0,\omega), \tag{23}$$

$$H_y(z=-0,\omega)=H_y(z=+0,\omega). \tag{24}$$

The integration constants C_{BW} and C_1 are obtained from

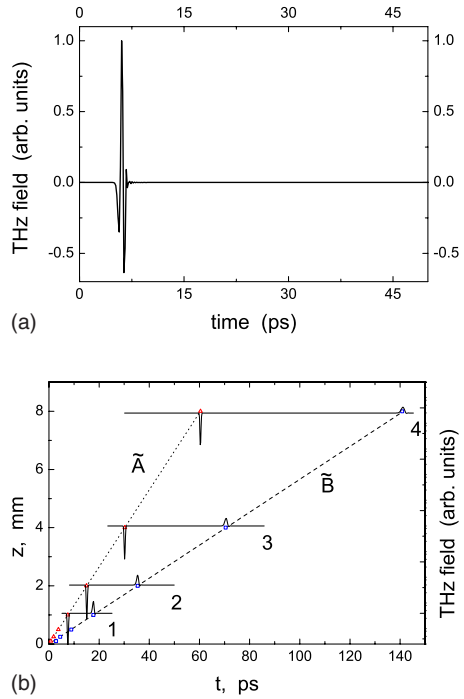

FIG. 2. (Color online) Top: Calculated wave form for terahertz far-field radiation emitting in anticollinear direction from semi-infinite medium. Bottom: Calculated wave forms for the EM field inside a semi-infinite medium (curves 1, 2, 3, and 4) from the continuous set of $E(z,t)$. The wave forms are shifted against each other in the z direction corresponding to the specified propagation lengths in the medium: curve 1 corresponds $z=1$ mm, curve 2 corresponds $z=2$ mm, curve 3 corresponds $z=4$ mm, and curve 4 corresponds $z=8$ mm. The lines $\tilde{A}$ and $\tilde{B}$ correspond to the calculated pulse positions. The medium parameters are taken for $LiNbO_3$

$$C_{BW}=C_1-\Xi, \tag{25}$$

$$-\frac{C_{BW}}{c_0}=\frac{C_1}{c}-\frac{\Xi}{v_g}, \tag{26}$$

where $\Xi\equiv\Xi(\omega)=-L_{coh}^{FW}L_{coh}^{BW}S(\omega)/\pi^2$. The propagating sum of radiation and radiationless fields inside a semi-infinite medium in the direction of the positive z axis is

$$E(z,\omega)=\Xi\left[\frac{c}{v_g}\frac{v_g+c_0}{c+c_0}\exp\left(i\frac{\omega}{c}z\right)-\exp\left(\frac{\omega}{v_g}z\right)\right], \tag{27}$$

and the radiation field emitting from the sample in the backward direction is

$$E(z,\omega)=\Xi\left(\frac{c}{v_g}\frac{v_g+c_0}{c+c_0}-1\right)\exp\left(i\frac{\omega}{c_0}z\right). \tag{28}$$

Comparing with the case of infinite nonlinear medium, the appearance of the interface boundary "linear-medium–nonlinear-medium" has resulted in the generation of a strong single cycle EM pulse (Fig. 2) of terahertz radiation emitted backward. The nature of this radiation phenomena is regarded to the reaction of nonlinear medium interface boundary to the creation of polarization charge $\rho_d=-\nabla\mathbf{P}^{NL}$.

2. Nonlinear slab

In the case of a slab, the continuity at the input interface, $z=0$, is added by the continuity of **E** and **H** fields at the interface, $z=L$ (output boundary of nonlinear slab), where L is the thickness of the nonlinear slab. These BCs determine the radiation propagating forward and backward from the slab. To fulfill the BCs, we match the general solution of Eq. (11) in a slab:

$$E_x(z,\omega) = C_1 \exp\left(i\frac{\omega}{c}z\right) + C_2 \exp\left(-i\frac{\omega}{c}z\right) + \frac{L_{coh}^{FW} L_{coh}^{BW} S(\omega)}{\pi^2} \exp\left(i\frac{\omega}{v_g}z\right), \tag{29}$$

where C_1 and C_2 are integration constants, with the solutions of the wave equation in free space on both sides of the slab.[46] These equations are simply the homogeneous form [Eq. (21)]. Solving the boundary value problem (BVP), we match the full solutions for the field inside the slab [Eq. (29)] with the radiation terahertz field propagating in the negative direction of the z axis [Eq. (21)] and the forward-irradiated THz field $E_x(z,\omega)$ into the right-hand half of free space at $z>L$,

$$E_x(z,\omega) = C_{FW} \exp\left[i\frac{\omega}{c_0}(z-L)\right]. \tag{30}$$

The values of the integration constants, $C_1 \equiv C_1(\omega)$, $C_2 \equiv C_2(\omega)$, $C_{BW} \equiv C_{BW}(\omega)$, and $C_{FW} \equiv C_{FW}(\omega)$, are determined from the BCs for the tangential components:

$$E_x(z=z_0-0,\omega) = E_x(z=z_0+0,\omega), \tag{31}$$

$$H_y(z=z_0-0,\omega) = H_y(z=z_0+0,\omega), \tag{32}$$

where z_0 defines the interface boundaries, $z_0=0$ or $z_0=L$, respectively. The conservation of the tangential components of the electric and magnetic fields [Eqs. (23)–(32)] leads to the following set of BVP linear equations presented in matrix form:

$$\begin{pmatrix} 1 & 1 & -1 & 0 \\ \frac{1}{c} & -\frac{1}{c} & \frac{1}{c_0} & 0 \\ \exp\left(i\frac{\omega}{c}L\right) & \exp\left(-i\frac{\omega}{c}L\right) & 0 & -1 \\ \frac{1}{c}\exp\left(i\frac{\omega}{c}L\right) & -\frac{1}{c}\exp\left(-i\frac{\omega}{c}L\right) & 0 & -\frac{1}{c_0} \end{pmatrix} \otimes \begin{pmatrix} C_1 \\ C_2 \\ C_{BW} \\ C_{FW} \end{pmatrix} = \Xi \begin{pmatrix} 1 \\ \frac{1}{v_g} \\ \exp\left(i\frac{\omega}{v_g}L\right) \\ \frac{1}{v_g}\exp\left(i\frac{\omega}{v_g}L\right) \end{pmatrix}. \tag{33}$$

The solution of this matrix equation gives the values of integration constants:

$$C_1 = \Xi\frac{\Delta_{C_1}}{\Delta}, \quad C_2 = \Xi\frac{\Delta_{C_2}}{\Delta}, \quad C_{BW} = \Xi\frac{\Delta_A}{\Delta}, \quad C_{FW} = \Xi\frac{\Delta_B}{\Delta}. \tag{34}$$

In Eq. (34), Δ is the determinant of the square 4×4 matrix in the left-hand side (lhs) of Eq. (33), and Δ_{C_1}, Δ_{C_1}, $\Delta_{C_{BW}}$, and $\Delta_{C_{FW}}$ are the determinants obtained from Δ by the replacement of corresponding columns by the rhs vector, respectively. The determinant Δ is

$$\Delta = \frac{(c+c_0)^2}{c_0^2c^2}\exp\left(-i\frac{\omega}{c}L\right) - \frac{(c-c_0)^2}{c_0^2c^2}\exp\left(i\frac{\omega}{c}L\right). \tag{35}$$

The other determinants are

$$\Delta_{C_1} = \frac{(v_g+c_0)(c+c_0)}{c_0^2cv_g}\exp\left(-i\frac{\omega}{c}L\right) - \frac{(v_g-c_0)(c-c_0)}{c_0^2cv_g}\exp\left(i\frac{\omega}{v_g}L\right), \tag{36}$$

$$\Delta_{C_2} = \frac{(v_g-c_0)(c+c_0)}{c_0^2cv_g}\exp\left(i\frac{\omega}{v_g}L\right) - \frac{(v_g+c_0)(c-c_0)}{c_0^2cv_g}\exp\left(i\frac{\omega}{c}L\right), \tag{37}$$

$$\Delta_{C_{BW}} = \frac{2(v_g-c_0)}{c_0cv_g}\exp\left(i\frac{\omega}{v_g}L\right) + \frac{(c+c_0)(c-v_g)}{c^2c_0v_g}\exp\left(-i\frac{\omega}{c}L\right) - \frac{(c+v_g)(c-c_0)}{c^2c_0v_g}\exp\left(i\frac{\omega}{c}L\right), \tag{38}$$

$$\Delta_{C_{FW}} = -\frac{(c+c_0)(c+v_g)}{c^2c_0v_g}\exp\left[-i\omega L\left(\frac{1}{c}-\frac{1}{v_g}\right)\right] + \frac{(c-c_0)(c-v_g)}{c^2c_0v_g}\exp\left[i\omega L\left(\frac{1}{v_g}+\frac{1}{c}\right)\right] + 2\frac{v_g+c_0}{cv_gc_0}. \tag{39}$$

The complex amplitudes for the forward and backward emitted terahertz fields outside the slab are given by the preexponential factors of Eqs. (21) and (30), respectively,

$$E_x(L+,\omega) = -\frac{c_0}{\pi^2 v_g}\frac{L_{coh}^{FW}L_{coh}^{BW}S(\omega)}{(c-c_0)^2\exp(i\omega L/c)-(c+c_0)^2\exp(-i\omega L/c)}\left\{(c+c_0)(c+v_g)\exp\left[-i\omega L\left(\frac{1}{c}-\frac{1}{v_g}\right)\right]\right.$$
$$\left.-(c-c_0)(c-v_g)\exp\left[i\omega L\left(\frac{1}{v_g}+\frac{1}{c}\right)\right]-2c(v_g+c_0)\right\}, \quad (40)$$

$$E_x(0-,\omega) = \frac{c_0}{\pi^2 v_g}\frac{L_{coh}^{FW}L_{coh}^{BW}S(\omega)}{(c-c_0)^2\exp(i\omega L/c)-(c+c_0)^2\exp(-i\omega L/c)}\left\{2c(v_g-c_0)\exp\left(\frac{i\omega L}{v_g}\right)+(c+c_0)(c-v_g)\exp\left(\frac{-i\omega L}{c}\right)\right.$$
$$\left.-(c+v_g)(c-c_0)\exp\left(\frac{i\omega L}{c}\right)\right\}, \quad (41)$$

where the notations $z=L+$ and $z=0-$ show the coordinates outside the slab, respectively. Solutions (40) and (41) converge to zero if the thickness of the nonlinear material $L \to 0$. They describe the field distributions at the output aperture that is used to find the field in a remote zone far from the slab. The inverse Fourier transform on Eqs. (40) and (41) returns the time domain wave forms of terahertz field emitted from the slab in collinear and anticollinear directions.

D. Terahertz radiation emitted into free space in the far field

The spatial distribution of the light emitted into free space from the input and output surfaces of a nonlinear slab can be treated within the framework of the standard diffraction theory[47] using the Huygens wavelet construction. The active volume inside a nonlinear crystal, where the conversion into terahertz occurs, forms a small cylinder with the apertures on both input and output surfaces of the order of $\sim S_0$, where S_0 is the pump beam cross section. The scalar term $E_x(\mathbf{r},\omega)$ of terahertz field at an observation point r in free space behind the slab is found after performing the following integration:

$$E_x(r,\omega) = -\frac{i\omega}{2\pi c_0}\int_{S_0} E_x(L+,\omega)\frac{\exp(ikr)}{r}\cos(\mathbf{n},\mathbf{r})dS_0, \quad (42)$$

where $E_x(L+,\omega)$ is the field at the output aperture calculated from Eq. (40). The integral in Eq. (42) is taken over the pump and/or terahertz beam aperture cross section S_0. The time domain wave form $E_x(\mathbf{r},t)$ is obtained from Eq. (42) using the Fourier transform. The field wave form at the remote point (distanced by r_D) is given by

$$E_{THz}(t) = E_x(r,t) = \frac{1}{(2\pi)^2 c_0}\int_{S_0}\frac{\cos(\mathbf{n},\mathbf{r})}{r}\frac{d}{dt}E_x\left(L+,t-\frac{r}{c_0}\right)dS_0. \quad (43)$$

Similarly, the terahertz field emitted by the slab in the backward direction is found from Eqs. (42) and (43), using $E_x(0-,\omega)$ calculated from Eq. (41) instead of $E_x(L+,\omega)$.

III. NUMERICAL CALCULATIONS, EXPERIMENTAL PROCEDURES, AND DISCUSSION

In this section, we compare the theoretical and experimental time domain and spectral properties of terahertz wave forms, which unambiguously reveal the physics of nonlinear conversion and establish the spatial localization of the source regions emitting terahertz waves.

We begin from the analysis of the evolution of wave forms of the terahertz field obtained within a gedanken experiment using a semi-infinite medium. Figure 2, top, depicts the wave form of the terahertz field radiated into free space in a far-field region in anticollinear direction, obtained after inverse Fourier transform of Eq. (28). It is seen that the calculated terahertz pulse emitted in the direction of negative z presents a single pulse of very few cycles whose position corresponds to $t=t_0-|z|/c_0$, where $|z|$ is the absolute value of the far-field distance and $t_0=0$ is the moment of pump pulse entry into semi-infinite medium. Figure 2, bottom, also shows the wave form of the EM terahertz field distribution inside the sample calculated from the inverse Fourier transformed expression [Eq. (27)]. There are only four wave forms shown from the continuously calculated set. The wave form pattern inside semi-infinite medium consists of two pulses $\tilde{A}$ and $\tilde{B}$ of opposite polarities and with fundamentally different behaviors on time. It is seen that the first pulse, named as $\tilde{A}$, propagates accordingly with $z=t_{\tilde{A}}c_0/n_{opt}$, whereas the second pulse, $\tilde{B}$, propagates along z as $z=t_{\tilde{B}}c_0/n_{THz}$. Another striking distinction is that pulse $\tilde{A}$ experiences almost no dispersion and absorption. These properties of pulse $\tilde{A}$ are determined by the respective quantities calculated for the pump pulse frequency ω_0. These two marked major features unequivocally demonstrate the nature of these two pulses. Pulse $\tilde{A}$ is related to the EM field of polarization charge propagating with the group velocity of pump pulse v_g. This field, pulse $\tilde{A}$, has the nature of a Coulomb field associated with moving polarization charge, rather than a radiation propagating field. Pulse $\tilde{B}$ demonstrates that its nature is related to an EM field at terahertz frequencies that is dispersed and absorbed during its propagation inside the medium. The properties of pulse $\tilde{B}$ prove that it is related to terahertz EMR generated at the entry interface boundary

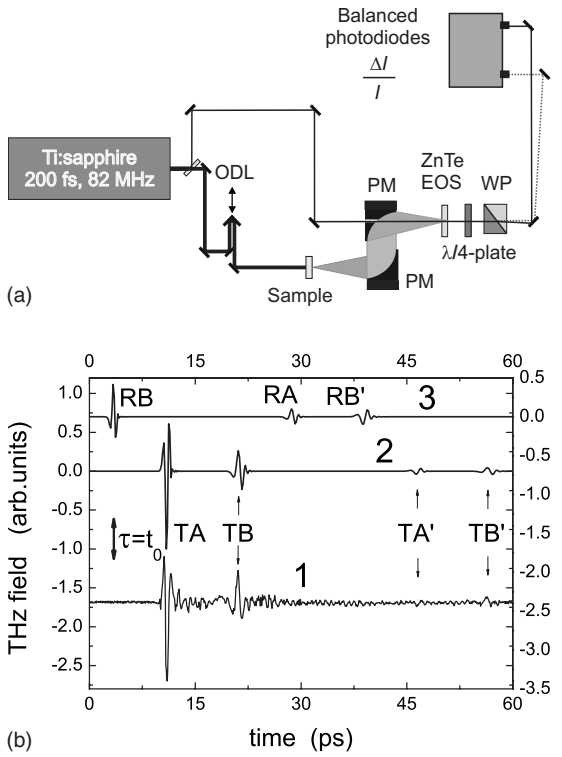

FIG. 3. Top: The sketch of experimental setup. Bottom: Comparison of experimental (curve 1) and theoretical (curves 2 and 3) terahertz wave forms emitted in a forward direction from the slab of $LiNbO_3$ of 1 mm thickness. Pulses labeled *TA-TB* and *TA′-TB′* correspond to forward emitted terahertz EMR and their first round-trip echo replicas, respectively. Theoretical curves 2 and 3 plot forward and backward emitted terahertz wave forms, respectively. The mark t_0 shows the time corresponding to the entry of the pump pulse into a nonlinear slab ($z=0$).

of pump pulse into semi-infinite medium. Vis-à-vis the above assertion, the occurrence of two fields inside a nonlinear medium has been misinterpreted within the NLWC model in Refs. 1, 2, and 18 and also widely accepted in textbooks, e.g., see Refs. 48–51. The crucial and unique evidence that unambiguously establishes the nature of this nonlinear phenomenon can only be obtained from studies of the reflection replica properties of $\tilde{A}$ and $\tilde{B}$ pulses. If the nature of pulse $\tilde{A}$ does indeed relate to the Coulomb field of the polarization charge, then after pulse $\tilde{A}$ reaches the output interface, it must change and generate a normal radiation terahertz pulse propagating with the velocity c, rather than v_g and also have other normal attributes. Notably, it must be established for both propagation directions, outward, into free space, and inward, back reflection from the interface into nonequilibrium medium. Below, we shall demonstrate this conversion in both ways, in experiments and theoretical calculations.

Our experimental investigations utilized $LiNbO_3$ and ZnTe crystals mounted in free space. Terahertz EMR was detected with a conventional setup shown in Fig. 3, top. $LiNbO_3$ and ZnTe samples had end face dimensions of $6 \times 10\ mm^2$ with a variety of lengths up to 4 mm. Optical excitation of the crystals was performed with 200 femtosecond pulses of a Ti:sapphire laser ($\lambda=850$ nm) focused to a spot whose size could be varied from 100 μm to 1.5 mm, and the average power was 300 mW. The $LiNbO_3$ crystal was mounted such that the c axis was parallel to the direction of polarization of the pump optical pulse. In the chosen geometry of $LiNbO_3$, the nonlinear polarization is determined by the largest component of the dielectric susceptibility tensor $\hat{\chi}^{(2)} \equiv \hat{\chi}^{(2)}_{33}$. Terahertz EMR radiating from the sample was collected and directed to the detector by a pair of parabolic mirrors (PM in Fig. 2, top). THz detection was accomplished using a free space electro-optic sampling cell[52–54] (EOSC) equipped with ZnTe crystal of the (110) facet orientation and 1 mm thickness—Fig. 2, top. To compare adequately the results of numerical calculations with experimental data, we compute theoretical wave forms and spectra taking into account the instrumental factors introduced by remote guiding of terahertz radiation by parabolic optics (Sec. II D) and detection in the EOSC. The detected terahertz wave form $S_{THz}(t)$ is the convolution of the signal emitted from the sample, $E_{THz}(t)$, with the instrumental factor $f(t)$,

$$S_{THz}(\tau) = \frac{\pi\epsilon_0}{c}\int_{-\infty}^{\infty} E_{THz}(t-\tau)f(t)dt$$

$$= \frac{\pi\epsilon_0}{c}\int_{-\infty}^{\infty} E_{THz}(\omega)f(\omega)\exp(i\omega\tau)d\omega. \quad (44)$$

The instrumental factor $f(t)$ results from the WVM between terahertz and probe pulses in the electro-optic material. It is described by the following relationship:[54]

$$f(\omega) = \frac{\pi\epsilon_0\omega_0^2}{c_0 k(\omega_0)}\exp[-2\beta(\omega_0)L]t_{12}(\omega)C_{opt}(\omega)$$

$$\times \frac{\exp[i\Delta k(\omega,\omega_0)L]-1}{i\Delta k(\omega,\omega_0)L}. \quad (45)$$

In Eq. (45), $k(\omega_0)$ is the real part of the complex wave vector κ, $\beta(\omega_0)$ is the attenuation coefficient, $\kappa(\omega)=k(\omega)+i\beta(\omega)$, $t_{12}(\omega)=2/[n(\omega)+1]$ is the Fresnel coefficient for terahertz EMR at frequency ω crossing the boundary air–electro-optic detector crystal, and

$$C_{opt}(\omega) = \int_{-\infty}^{\infty} E_{\text{probe}}(\omega'-\omega_0)E_{\text{probe}}(\omega'-\omega_0-\omega)d\omega'. \quad (46)$$

Equation (46) is the autocorrelation function of the probe pulse electric field $E_{\text{probe}}(\omega'-\omega_0)$; $\omega'-\omega_0$ is the detuning relative to the central probe pulse frequency ω_0.

To compute Eqs. (40) and (41) numerically, we use the Sellmeier equations for the evaluation of v_g: in $LiNbO_3$,[55]

$$n(\lambda) = \left(4.582 - \frac{0.099\,169}{0.044\,432-\lambda^2} - 0.021\,95\lambda^2\right)^{1/2}, \quad (47)$$

and for ZnTe,[56]

$$n(\lambda) = \left(4.27 + \frac{3.01\lambda^2}{\lambda^2 - 0.142}\right)^{1/2}. \quad (48)$$

The value of c is calculated using the expression for the dielectric constant at terahertz frequencies, $\epsilon(\omega)$, in the approximation of the single TO-oscillator model related to the lowest frequency of the infrared active phonon modes of A_1 symmetry:[57,58]

$$\epsilon(\omega) = \epsilon_\infty + \frac{S\omega_{\mathrm{TO}}^2}{(\omega_{\mathrm{TO}}^2 - \omega^2) - i\omega\Gamma}, \quad (49)$$

where ϵ_∞=4.03, S=23.9, ω_{TO}=7.68 THz, and Γ=0.93 THz are the best fit parameters to the experimental data for $\epsilon(\omega)$ in $LiNbO_3$.[58] For ZnTe, we use Eq. (49) with the following parameters: ϵ_∞=7.44, S=2.58, ω_{TO}=5.32 THz, and Γ=0.025 THz.[54] For numerical calculations of terahertz wave forms, we use Eqs. (40)–(43) corrected for the instrumental factor of EOSC [Eqs. (44) and (45)] using $LiNbO_3$ parameters included in Eqs. (47) and (49) and ZnTe parameters included in Eqs. (48) and (49).

The wave form of terahertz radiation calculated for, and measured from, a 1 mm thick sample of $LiNbO_3$ placed in free space is shown in Fig. 3, bottom. First, we describe the structure of the terahertz wave form and its variation with experimental conditions, such as focusing and sample positioning. The terahertz wave form consists of several separated pulses. Two leading pulses, *TA* and *TB* (curves 1 and 2, Fig. 3, bottom), represent terahertz EMR emitted during a single flight of the pump pulse and are consistent with the observation made in Ref. 19. Prefix *T* here indicates the transmission geometry, i.e., terahertz EMR emitted from the slab in the forward direction. Each pulse starts with intensive bipolar oscillations defining the overall shape of the spectral envelope. In the experimental wave form, it is followed by weak prolonged oscillations related to various specific spectroscopic details, such as the residual water absorption of the free space atmosphere, etc. The pulses *TA* and *TB* have largely opposite signs. Curve 2 of Fig. 3, bottom, presents the calculated wave form for the $LiNbO_3$ sample of the same thickness. Numerical calculations are made for the sample placed *in vacuo* and, therefore, the theoretical wave forms do not include the oscillations in the tail of the pulse introduced by atmospheric residual gases and water vapor absorption. From a comparison of wave forms 1 and 2 of Fig. 3, bottom, a good fit of the theoretical wave form to the experimental graphs for all of the major features is evident. To measure the thickness dependence of terahertz DFG wave forms on thickness L, the samples were placed on a fixed base plate that provided a common origin in time scale, with an accuracy better than ±10 fs. The series of terahertz wave forms was recorded successively using the sample set of different thicknesses ranging from 0.2 up to 4 mm. For each wave form, we find that the positions of the forward propagating pulses after a single round-trip, *TA* and *TB*, are referable to *TA′* and *TB′*, which are the first round-trip echo replicas. For each thickness of measured samples, we calculate the wave form and then determine the positions of peaks *TA*, *TB*, *TA′*, and *TB′*. Figure 4 plots the fan diagram of pulse positions as a function of slab thickness. The position of pulse *TA* follows the time of flight of the pump pulse, $t_A = Ln_{opt}(\omega_0)/c_0$. The temporal position of the pulse *TB* corresponds to $t_B = Ln_{THz}/c_0$, that is, the time of flight of the terahertz EMR pulse across the slab. The relative time of flight between pulses *TA* and *TB* is $\Delta t_{A\text{-}B} = L(n_{THz} - n_{opt})/c_0$. As stated in Sec. I, these data themselves do not deliver conclusive evidence on the nature of the *TA* and *TB* pulses. However, since both models had in their theoretical footing the same form of the Maxwell's equations, their conclusions should have been consistent regardless of whether they was built on a harmonic waves approximation[2,6,8] or used the time domain treatment based on the formation and propagation of wave packets (Sec. II). Therefore, to identify the correlations between these two interpretations, it is important to investigate the properties of DFG wave packet conversion in as detailed a manner as possible. In order to search for such evidence, we turn to the analysis of other properties of DFG EMR that, so far, have not been addressed.

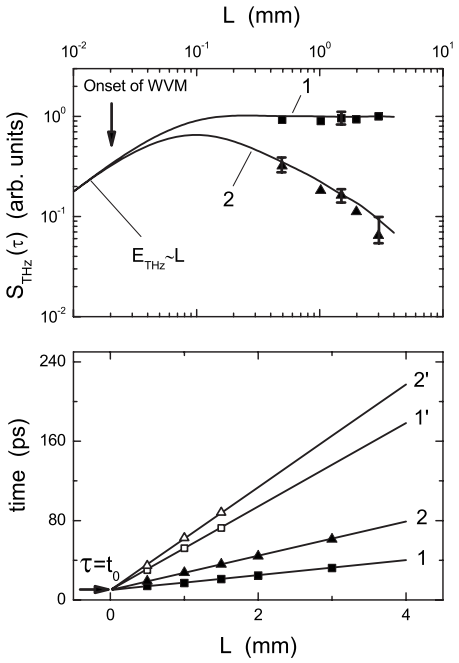

FIG. 4. Bottom: Fan diagram showing positions of peaks (1) *TA*, (2) *TB*, (1′) *TA′*, and (2′) *TB′* as functions of slab thickness *L*. Top: Dependencies of the terahertz field peak amplitude on slab thickness for pulse *TA* (1) and pulse *TB* (2). Experimental points are shown by squares and triangles. Solid curves 1, 2, 1′, and 2′ show theoretical dependencies.

The amplitude dependence on thickness for forward emitted EMR, shown in Fig. 4, demonstrates linear growth of the main terahertz pulse amplitude at thicknesses $L < L_{coh}^{FW}$. At a certain thickness, corresponding to the onset of WVM, the main pulse splits into two pulses labeled as *TA* and *TB*. The amplitude of pulse *TA* saturates with L and remains largely constant, irrespective of further increase of slab thickness. Unlike pulse *TA*, the amplitude of pulse *TB* strongly falls with L. The results of spectral analysis of pulse *TA* and *TB* obtained by Fourier transform of the time-domain wave form sampled within 10 ps of each pulse separately are shown in

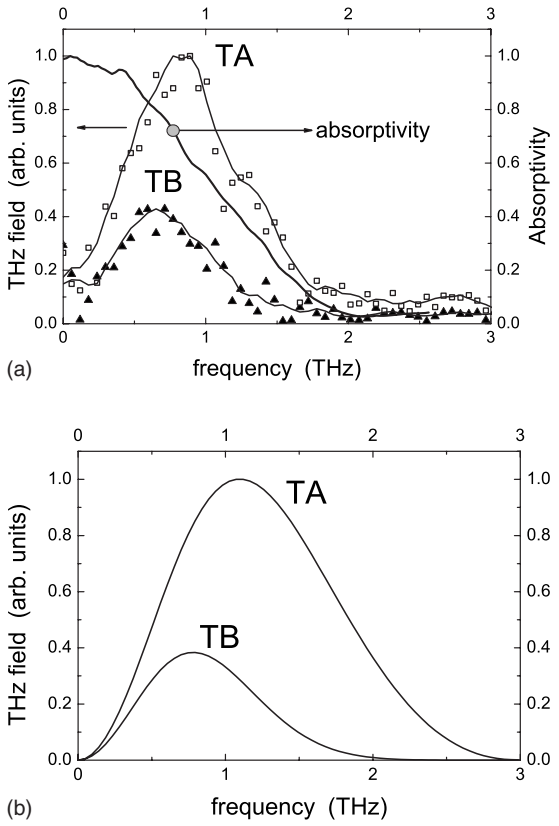

FIG. 5. Top: Experimental terahertz spectra of *TA* (curve *TA*) and *TB* (curve *TB*) pulses obtained for $LiNbO_3$ sample of $L=1$ mm. The curve marked "absorptivity" shows the dependence of the absorptivity in $LiNbO_3$ defined as the ratio of transmitted to incident electric field amplitudes. Bottom: Theoretical terahertz spectra of *TA* and *TB* pulses calculated for the $LiNbO_3$ sample with $L=1$ mm.

Fig. 5. The spectral envelope of pulse *TB* is shifted by 200 GHz to lower frequencies relative to spectrum of *TA*. It is known that the absorption coefficient in the terahertz band normally rises with frequency.[58] Theoretical spectra calculated with the complex refractive index taken from Ref. 59 show the shift of the *TB* spectrum close to 200 GHz and have approximately the same amplitude ratio *TB*/*TA* as that measured experimentally—Fig. 5. Therefore, the shift of pulse *TB* spectrum is explained as the result of reabsorption during propagation of the pulse *TB* across the sample. Figures 4 and 5 emphasize that the spectrum of pulse *TA* remains independent of thickness within the measurement accuracy. The calculated spectra of pulses *TA* and *TB*—Fig. 5—correspond with a good accuracy to the results of experiment. The strong reduction of amplitude of pulse *TB* with thickness may be regarded as a signature of strong attenuation and broadening of the pulse *TB* inside the slab. The amplitude dependencies of pulses *TA* and *TB* could still be treated within the framework of a qualitative NLWC model[2,6] if the pulse *TB* was attributed to HW and the *TA* pulse was related to IHW. In this case, the observed behavior would result from the differences in the complex propagation constants, absorption coefficients, and refractive indices for HW and IHW, respectively.

To identify a convincing proof, we address the properties of the echo replicas of pulses *TA* and *TB*, with the pulses *TA′* and *TB′* following the leading pair *TA*-*TB*. The key significance of the data extracted from the properties of echo replicas is motivated by the idea that, for spatially separated sources (TR model), the echo replicas should show characteristic modifications of properties in comparison with the properties of pulses from direct flight, whereas for the pulses generated within the same volume adjacent to the input surface (NLWC model), the echo replicas should keep, at least, the same structure and amplitude ratio. Moreover, if, as suggested in Ref. 2, the so-called IHW does indeed represent a real propagating wave (created by nonlinear conversion along with HW), it must keep its "extraordinary" properties after the reflection from boundaries. These are that the frequency is equal to the conversion frequency and the complex wave velocity is equal to the group velocity of the pump pulse. From Fig. 4, showing the fan diagram of arrival times for the main pulses and their reflection replicas, we can see that time positions for the *TB′* replica behave consistently with the properties of the *TB* pulse. Being reflected sequentially from the output and input interfaces, the pulse *TB′* acquires a round-trip delay $2Ln_{THz}/c_0$ in addition to the arrival time $t_{B'}=3Ln_{THz}/c_0$. The arrival time of flight for the *TA′* pulse, $t_{A'}$, includes the time of flight of *TA*, Ln_{opt}/c_0, accomplished with a round-trip time of the terahertz pulse, $2Ln_{THz}/c_0$, leading to the total arrival time of *TA′* pulse $t_{A'}=Ln_{opt}/c_0+2Ln_{THz}/c_0$. This is confirmed by both the experiments and theory—Fig. 3, bottom. To our knowledge, this striking result has not yet been reported elsewhere. It casts a decisive vote in favor of the TR model, providing the crucial evidence for conversion of the polarization charge field into a pulse of terahertz EMR at the exit from the slab. This unequivocally establishes the physical meaning of the inhomogeneous solution of the wave equation [the third term in rhs of Eq. (29)] as the field of moving charge, the polarization charge, rather than an EM wave component related to the so-called IHW all the way through (see, e.g., Refs. 2 and 6). This directly shows that conversion of the charge field into a bunch of propagating EM waves occurs at the entry and exit boundaries due to the radiation mechanism at charge "start-stop" motion.[21,25]

Another argument in favor of the TR mechanism is inferred from Fig. 3, bottom, where a striking inversion of the amplitude ratio from $TA/TB \gg 1$ to $TA'/TB' \lesssim 1$ (Fig. 3, bottom) is also evident. It shows that after a seemingly simple round-trip, the terahertz EMR pulses demonstrate a striking change of amplitude ratio: Compare the ratio of *TA* to *TB′* and the ratio *TA′* to *TB′* in Fig. 3, bottom. Had the sources of pulses *TA* and *TB* been localized within the same spatial region of the nonlinear slab from the front surface, as interpreted in the NLWC model,[2,6] then both *TA* and *TB* pulses would bounce back and forth keeping at least the same amplitude ratio. From the data of Fig. 3, bottom, we can estimate the ratio of formation lengths for forward to backward emitted terahertz EMRs. Classification of the backward emitted pulses is shown by using *R* to mark their affiliation to the backward (reflection) direction. Since the field amplitude is proportional to the value of the formation-coherence length, we obtain the ratio $\eta=TB/RB \sim L_{coh}^{FW}/L_{coh}^{BW}$. It is clear that the

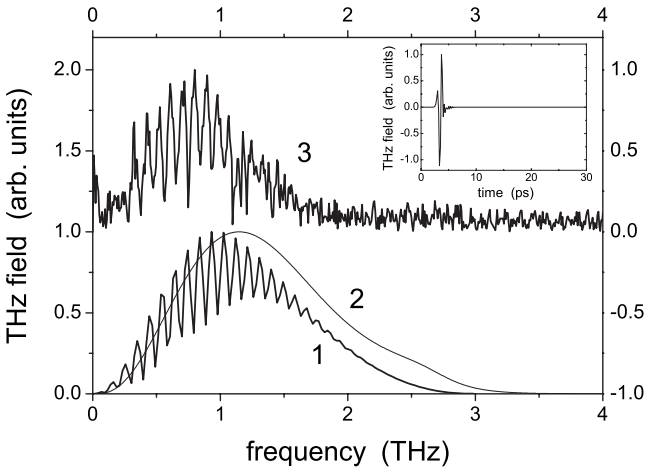

FIG. 6. Terahertz spectra calculated for $LiNbO_3$ samples for (1) $L > L_{coh}^{FW}$ and (2) $L < L_{coh}^{FW}$. The inset shows the time domain wave form related to spectrum (2). The terahertz spectrum (3) shows the experimental spectrum of *TA* and *TB* pulses obtained for $L > L_{coh}^{FW}$.

ratio TA/TB is a measure of absorption in the slab. Assuming that the absolute value of peak amplitude remains the same on both interfaces, we recover the amplitude of the *TB* pulse at $z = 0 + TB|_{z=0+} \sim TA$. Then, from Fig. 4, we find $L_{coh}^{FW}/L_{coh}^{BW} \simeq 2.5$; this is in a good agreement with the calculated value of $\eta \approx 2.46$.

Maker *et al.*[9] have demonstrated strong oscillations of SHG intensity as the angle of sample position with respect to the direction of pump propagation is changed. The theory for these oscillations has been developed in Ref. 8, and it is now widely accepted (see, e.g., Refs. 49 and 50) that it is the interference of HW and IHW at the conditions of stationary excitation, according to Ref. 8, that leads to the oscillatory behavior of the intensity of the converted wave as function of sample thickness.[9] These oscillation patterns have formed the basis of a widely used method to measure the absolute values of second-order nonlinear optical coefficients. The oscillatory factor $\propto \sin^2 \Phi$, where $\Phi = \pi L/2L_{coh}^{FW}$.[8,9] We note that this form of oscillatory factor Φ can be transformed to the form $\Phi = \frac{1}{2}\omega_{THz}\Delta t_{A\text{-}B}$ using Eq. (18). To verify this assertion, we compare the spectra of the complete structure of the twin pulses, *A* and *B*. Figure 6 plots experimental and theoretical spectra of the wave form including the *TA* and *TB* twin pulses. Both the theory and experiments demonstrate very similar, well pronounced periodic oscillations that follow exactly the proportionality to $\sin(\frac{1}{2}\omega_{THz}\Delta t_{A\text{-}B})$. As stated above, this result demonstrates the identity of these oscillations with Maker fringes.[9] This clearly shows that the nature of Maker oscillations is due to interference of TR components emanating from the entry and exit interface boundaries. If the thickness of the sample becomes less than L_{coh}^{FW}, the twin wave forms merge into a single pulse wave form (inset of Fig. 6). Under these conditions, the spectrum oscillations disappear, and the curve becomes smooth (curve 2 in Fig. 6).

The final part of this section briefly discusses the results obtained from the ZnTe sample where the conditions $L_{coh}^{FW} \gtrsim L$ are met for a substantial fraction of terahertz frequencies $F \lesssim 2$ THz with sample length $L \sim 1$ mm. Figure 7 shows the

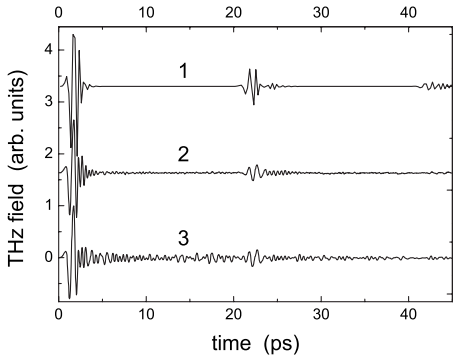

FIG. 7. Calculated (1) and experimental (2) and (3) THz wave forms for the ZnTe crystal (110), $L = 1$ mm. Wave forms (2) and (3) were recorded at environment purged with dry nitrogen gas and ambient air environment, respectively.

experimental and theoretical wave forms measured and calculated for this sample. This case clearly demonstrates a hybrid mechanism of terahertz EMR where the conditions $L < L_{coh}^{FW}$ are met for the low frequency part of the terahertz spectrum, $F \lesssim 2$ THz. For the upper frequencies, $F > 2$ THz, L_{coh}^{FW} quickly falls. The mechanism of terahertz generation changes over this region to the case of TR, with the conditions $L > L_{coh}^{FW}$. The overall pulse shape appears more complex, if it is compared with the case of $L_{coh}^{FW} \gg L$ (the calculated wave form shown in the inset of Fig. 6). Part of the theoretical curve corresponding to the reflection replica (the second pulse of curve 2 in Fig. 7) shows a fine substructure of the replica pulse, which apparently relates to a chirp of the terahertz pulse during the round-trip propagation inside the ZnTe sample.

The physics of terahertz wave generation during nonlinear coherent three-wave interaction is fundamentally different from the framework of NLWC model which is usually treated as the periodic series of successive constructive and destructive coherent nonlinear wave transformations (transformations from the pump wave to converted wave and vice versa), each of which occurs on the scale of L_{coh} in the bulk of medium (see, e.g., Refs. 1, 49, and 50). It is quite clear that, due to the coherent nature of the nonlinear wave transformation, each constructive coupling event in the bulk should generate a pulse of terahertz radiation with firmly fixed phase and/or time shift with respect to the preceding event. Then, the total terahertz wave form generated by a sample of thickness L in the collinear direction would show a series (i.e., a comb) of pulses with "quantized" delays of number $L/L_{coh}+1$. The reason why this "tentative" speculation fails the test in the time domain is that nonlinear wave coupling comes into play through nonlinear polarization that, of course, leads to formation of a polarization charge [Eqs. (2) and (3)], which moves with the velocity of the pump light in the medium. It is the radiation of this charge that determines the mechanism of wave conversion at the conversion frequency, rather than the series of mutual *back and forth* nonlinear wave transformations. What really matters is the character of the polarization charge motion that is, of course, uniform in the bulk. Thus, in the bulk, the charge can radiate if and only if its velocity exceeds the phase velocity of the

converted wave. This is the VC radiation mechanism, which is the fundamentally noncollinear coherent radiation from the entire path of pump pulse considered as a single radiator. Otherwise, and, in particular, in the collinear direction, the radiation from the bulk is strictly forbidden—Sec. II B, Eq. (17). In the collinear direction (as shown above in Secs. II C and III), the polarization charge can only radiate at the moment of its formation and of its extinction within the scale of L_{coh} at the entry and exit boundaries, respectively. Under the condition $L_{coh} \gtrsim L$, these radiation events simply overlap: This can be interpreted as the collinear "phase matching" radiation. However, the properties of the radiation at such overlap differ in some respects from the radiation at perfect PMCs that require the degeneration of velocities of moving source, v_g, and conversion wave, c, at the frequencies of the pump and conversion, $v_g(\omega_p)=c(\omega)$.

IV. CONCLUSIONS

To summarize, the reported experimental and theoretical results have unambiguously established the mechanism of terahertz DFG with short optical pulses. With a nonlinear slab, the burst of terahertz EMR is fired twice: at the moment of formation of the polarization charge, due to the nonlinear coupling of the fields of the short pump pulse traversing the boundary between the linear and nonlinear media, and at the moment of extinction of the polarization charge at the exit of the pump pulse from the slab. This mechanism of TR with optical pulses is very similar to that discussed within the framework of the so-called Tamm problem for radiation caused by the start-stop motion of charged particles in a uniform medium. It has been shown that, if the coherence length becomes comparable with the thickness of a nonlinear medium, TRs from both interfaces overlap and they merge into a single bunch of collinear PM radiation. Efficient broadband TR terahertz generation can be obtained at the interfaces of free space and a nonlinear sample with a high value of $\hat{\chi}^{(2)}$, even if the coherence length is small. TR causes Maker oscillatory behavior that is due to interference between the coherent terahertz EMR generated at the input and output boundaries. These interference fringes are different in nature from the interference arising from the round-trips (multiple reflections) of the terahertz pulse itself. The results of theoretical calculations fully agree with the experimental data. Although the major part of this paper is devoted to difference frequency generation (DFG), related to the radiation at terahertz frequencies, it is attributable to a much broader family of nonlinear phenomena.

ACKNOWLEDGMENTS

The authors would like to acknowledge financial support from the Department of Trade and Industry National Measurement System Policy Unit in the UK, The Royal Society, UK, the Ministry of Education and Science of Armenia (Contracts No. 840 and No. INTAS-01-0397), the Russian Foundation for Basic Research (Grant No. 05-02-17770) and the grant for innovations support from the Russian Academy of Sciences.

APPENDIX: NONLINEAR WAVE CONVERSION MODEL: LINEARIZED APPROACH

Obtaining analytical solutions of the wave equation, for various reasons, is not always achievable. A linearized approach to the wave equation[43,44,59] has been known for a long time, often termed as the paraxial approximation. It has been applied to the wave equation with nonlinear source term as early as 1962,[1,2] and this has been followed by numerous further publications, e.g., see Refs. 6–10 Below, we briefly outline the scheme of linearization aiming to draw up the relevant comparisons and conclusions to the subject of this paper. The treatment of the set (2) and (3) usually proceeded within the framework of the slow varying envelope amplitude approximation (SVEA):

$$\mathbf{E}_i(\mathbf{r},t) = \mathbf{e}_i A_i(\mathbf{r},t)\exp[i(k_{0i}z - \omega_{0i}t)] + \text{c.c.}, \tag{A1}$$

where $\mathbf{e}$ is the polarization vector, $A_i(\mathbf{r},t)$ is the field envelope assumed to be slow varying on the scale of λ_{0i} and ω_{0i}, ω_{0i} is the carrier frequency, and k_{0i} is the carrier wave vector. Index i denotes the pump waves as $i=pj,pk$ and the converted wave as $i=c$. Then, instead of Eqs. (8) and (9), the following equation is obtained from Eq. (2) using Eq. (A1) and the Fourier transform of Eq. (2):

$$\begin{aligned}\nabla_\perp^2 A_c(\mathbf{r},\omega-\omega_{0c}) + \frac{\partial^2 A_c(\mathbf{r},\omega-\omega_{0c})}{\partial z^2} + 2ik_{0c}\frac{\partial A_c(\mathbf{r},\omega-\omega_{0c})}{\partial z} \\ + [k^2(\omega) - k_{0c}^2]A_c(\mathbf{r},\omega-\omega_{0c}) \\ = -i\omega\mu_0\sigma(\omega)A_c(\mathbf{r},\omega-\omega_{0c}) - \mu_0\omega^2 P^{NL}(\mathbf{r},\omega)e^{-ik_{0c}z}.\end{aligned} \tag{A2}$$

The last term in lhs of Eq. (A2) describes smearing of the pulse envelope $A(\mathbf{r},t)$ due to the group velocity dispersion (GVD). Using the assumption of slow varying amplitude on the scale of λ, the following approximation is used:

$$\frac{\partial^2 A_c(\mathbf{r},\omega-\omega_{0c})}{\partial z^2} \ll k_{0c}\frac{\partial A_c(\mathbf{r},\omega-\omega_{0c})}{\partial z}. \tag{A3}$$

The following linearized wave equation is normally used in all practical treatments of NLWC:

$$\begin{aligned}\nabla_\perp^2 A_c(\mathbf{r},\omega-\omega_{0c}) + 2ik_{0i}\frac{\partial A_c(\mathbf{r},\omega-\omega_{0c})}{\partial z} \\ + [k^2(\omega) - k_{0c}^2]A_c(\mathbf{r},\omega-\omega_{0c}) \\ = -i\omega\mu_0\sigma(\omega)A_i(\mathbf{r},\omega-\omega_{0c}) - \mu_0\omega^2 P^{NL}(\mathbf{r},\omega)e^{-ik_{0c}z}.\end{aligned} \tag{A4}$$

Equation (A4) is the paraxial nonlinear Helmholtz equation with inclusion of losses due to free carrier absorption [the first term in the rhs of Eq. (A4)]. After putting the GVD term in power series form, Eq. (A4) is transformed into the formal equivalent to the Schrödinger equation and is used for the treatment of many phenomena in optics and quantum optics, including short pulse propagation in Kerr medium,[4,5,12–14,59–61] The first term of Eq. (A4) describes the variation of the amplitude in the transverse plane to the propagation direction. Neglecting GVD term and applying Eq. (A4) to the one-dimensional problem of collinear radia-

tion lead to the linearized wave equation. If we assume that the region of interest, where nonlinear wave conversion occurs, is restricted within the size of the confocal parameter around the origin of coordinate $z=\pm z_0$ (this assumption is equivalent to the case when the thickness of the nonlinear slab $L<z_0$), then Eq. (A4) is reduced to

$$\frac{\partial A_c(z,\omega-\omega_{0c})}{\partial z} = -\frac{\alpha_c}{2}\frac{\omega}{\omega_{0c}}A_c(z,\omega-\omega_{0c}) - i\frac{1}{2}\sqrt{\frac{\mu_0}{\epsilon_0\epsilon}}\frac{\omega^2}{\omega_{0c}}P^{NL}(z,\omega)e^{-ik_{0c}z}, \quad \text{(A5)}$$

where $\alpha_c=\sigma\sqrt{\mu_0/\epsilon_0\epsilon_c}$ is the absorption coefficient of the generated field. With obvious assumption $\omega\sim\omega_{0c}$, Eq. (A5) is transformed to the equation used in the original papers[1,2,18,48] followed by a huge number of papers treating second harmonic generation (SHG), sum frequency generation (SFG), and difference frequency generation (DFG) or optical rectification (OR), if a single pump is used. This approach has been replicated in many textbooks (e.g., see Refs. 48–51). Using the expression for nonlinear polarization for OR/DFG is considered using the linearized form of the wave equation:[48–51]

$$\frac{dA_c(\omega,z)}{dz} = -\frac{\alpha_c}{2}A_c(\omega,z) - i\omega\sqrt{\frac{\mu_0}{\epsilon}}d_{ijk}A_{pj}(\omega-\omega_{pj},z)A^*_{pk}(\omega-\omega_{pk},z)\exp(-i\Delta kz)\exp\left(-\frac{\alpha_j+\alpha_k}{2}z\right) \quad \text{(A6)}$$

where $2d_{ijk}=\chi^{(2)}_{ijk}$, $\Delta k=k_{pj}-k_{pk}-k_{0c}$, and α_j and α_k are the absorption coefficients for the components of pump fields, respectively. Equation (A6) is a simple linear differential equation of the first order that is easily integrated. The solution of Eq. (A6) requires only single BC at the entry interface of nonlinear medium. Most of the papers and textbooks use the trivial zero BC at $z=0$: $A_c(\omega,z)|_{z=0}=0$. Such a choice of BC is usually justified by the argument that strictly at the interface $z=0$, because of zero length of nonlinear medium, no generation of converted field is able to build up. With such choice of BC, the solution of Eq. (A6) for the field amplitude is given by

$$A_c(z,\omega) = \frac{i\omega\sqrt{\frac{\mu_0}{\epsilon}}d_{ijk}A_{pj}A_{pk}}{(\Delta k)^2+\left(\frac{\alpha_j+\alpha_k-\alpha_c}{2}\right)^2}\left[-i\Delta k - \frac{\alpha_j+\alpha_k-\alpha_c}{2}\right]\exp\left(-\frac{\alpha_c}{2}z\right)\left\{1-\exp\left[-\left(i\Delta k + \frac{\alpha_j+\alpha_k-\alpha_c}{2}\right)z\right]\right\}. \quad \text{(A7)}$$

The quantity

$$A_c(z,\omega)A^*_c(z,\omega) = \frac{\omega^2\left(\frac{\mu_0}{\epsilon}\right)d^2_{ijk}A^2_{pj}A^2_{pk}}{(\Delta k)^2+\left(\frac{\alpha_j+\alpha_k-\alpha_c}{2}\right)^2}\exp(-\alpha_c z)\left\{1 - 2\cos(\Delta kz)\exp\left[-\frac{\alpha_j+\alpha_k-\alpha_c}{2}z\right] + \exp[-2(\alpha_j+\alpha_k-\alpha_c)z]\right\} \quad \text{(A8)}$$

determines the power of converted wave. It is easy to see that the power, proportional to the quantity expressed by Eq. (A8), oscillates with z as $\cos(\Delta kz)$, if $\Delta k\neq 0$. The power oscillations decay with z with the composite absorption coefficient $\Delta\alpha=\alpha_j+\alpha_k-\alpha_c$ and the power of generated wave decays with the absorption coefficient α_i. Using the notations for the power densities,

$$\frac{P_c}{S} = \frac{1}{2}\sqrt{\frac{\mu_0}{\epsilon_c}}A_cA^*_c\frac{P_{pj}}{S} = \frac{1}{2}\sqrt{\frac{\mu_0}{\epsilon_j}}A_{pj}A^*_{pj}\frac{P_{pi}}{S} = \frac{1}{2}\sqrt{\frac{\mu_0}{\epsilon_k}}A_{pk}A^*_{pk}, \quad \text{(A9)}$$

we obtain the widely used formula (see, e.g., Ref. 62) for the power conversion efficiency for nonlinear generation and/or conversion at three-wave interaction process at phase matching condition, $\Delta k=0$, on the length of nonlinear medium z:

$$P_c = \frac{8}{S}\omega^2\left(\frac{\mu_0}{\epsilon_0}\right)^{3/2}\frac{P_{pj}P_{pk}}{n_in_jn_k}(d_{ijk})^2z^2 \times\exp(-\alpha_c z)\frac{\left[1-\exp\left(-\frac{\Delta\alpha z}{2}\right)\right]^2}{\left(\frac{\Delta\alpha z}{2}\right)^2}. \quad \text{(A10)}$$

The apparent simplicity of the linearized wave equations [Eqs. (A6)–(A10)] is bought at a certain price. First of all, it must be stated that Eqs. (A7)–(A10) seem to establish the generation of EMR due to nonlinear coupling of EM fields everywhere in the medium. This is strikingly inconsistent with the exact result [Eq. (17)] of Sec. II B. Another major drawback of the linearized approach is demonstrated in Fig. 8. Figure 8 plots the wave forms calculated for a semi-infinite medium using inverse Fourier transform of Eq. (A7). Although it produces a twin pulse structure of EM field pattern inside the medium, in marked comparison with Fig. 2, this reveals physically unreasonable properties of these twins. Two more striking misfits are in predicted position for pulse $\tilde{B}$ and pulse $\tilde{A}$ whose propagation through medium is predicted with infinitely high velocity.

The major difficulties stem from the reduction of the order of the differential equation that leads to the loss of correct solution. The approach based on the scheme of SVEA [Eq. (A1)] and linearization [Eq. (A3)] of Maxwell equations leads to Eqs. (A6)–(A10). The linearized equation of reduced order, the first-order differential equation [Eq. (A6)], does not require the BC at the output interface. Without going into the details of legitimacy of the widely used assumption

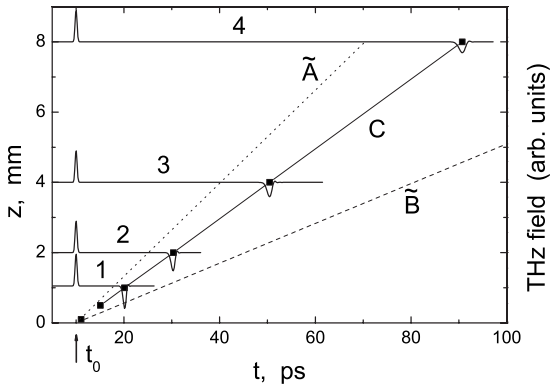

FIG. 8. THz wave forms calculated for a semi-infinite medium within the scheme of a linearized SVEA approximation (the medium parameters are taken for $LiNbO_3$). Similarly to Fig. 1, the wave forms are shifted against each other in the z direction corresponding to the specified propagation lengths in the medium: curve 1 corresponds $z=1$ mm, curve 2 corresponds $z=2$ mm, curve 3 corresponds $z=4$ mm, and curve 4 corresponds $z=8$ mm. The lines $\tilde{A}$ and $\tilde{B}$ follow $z=t_{\tilde{A}}c_0/n_{opt}$ and $z=t_{\tilde{B}}c_0/n_{THz}$, respectively. The line C is the guideline for the second pulse positions.

$A(z,\omega)|_{z=0}=0$ (e.g., used in Refs. 11, 15, 16, and 63), we state that the absence of the BC at the output interface ultimately leads to the wrong physics: The solution simply does not "feel" the output boundary. It is also true, even if the correct choice of the BC at the entry interface, the continuity of tangential components for **E** and **H** vectors, applies. As a consequence of this, there is a misleading behavior of the power of the generated wave oscillations with propagation distance in nonlinear medium z as $\cos(\Delta kz)$ at arbitrary WVM $\Delta k \neq 0$. Furthermore, being applied to calculate the time domain wave form pattern, Eq. (A7) generates two pulses with physically unreasonable properties. The field wave form emitted out of a slab in collinear direction is Eq. (A7) multiplied by the Fresnel transmission coefficient $T=4n/(n+1)^2$. In Ref. 63, Eq. (A7) has been applied to the analysis of a structure of terahertz wave forms in ZnTe measured with excitation wavelengths $\lambda \sim 1.07-1.24$ μm. As it is shown above, particularly in Fig. 8, widely used formulas (A6)–(A10), when applied to the description of nonlinear optics phenomena, give clearly wrong answers on the details of time-frequency domains kinetics. It creates even more confusions to the understanding of optical phenomena when one deals with short pulses, e.g., single or few cycles pulses. Therefore, for the correct description of the physics related to optical nonlinearities with single or few cycles EM pulses, the full set of Maxwell', equations must be deployed without the use of the linearization procedure and the SVEA approximation.

*nick.zinovev@durham.ac.uk

[1] J. A. Armstrong, N. Bloembergen, J. Ducuing, and P. S. Pershan, Phys. Rev. **127**, 1918 (1962).
[2] N. Bloembergen and P. S. Pershan, Phys. Rev. **128**, 606 (1962).
[3] M. Bass, P. A. Franken, J. F. Ward, and G. Weinreich, Phys. Rev. Lett. **9**, 446 (1962); M. Bass, P. A. Franken, and J. F. Ward, Phys. Rev. **138**, A534 (1965).
[4] T. Brabec and F. Krausz, Rev. Mod. Phys. **72**, 545 (2000).
[5] T. Brabec and F. Krausz, Phys. Rev. Lett. **78**, 3282 (1997).
[6] D. A. Kleinman, Phys. Rev. **128**, 1761 (1962).
[7] R. C. Miller, D. A. Kleinman, and A. S. Savage, Phys. Rev. Lett. **11**, 146 (1963).
[8] J. Jerphagnon and S. K. Kurtz, J. Appl. Phys. **41**, 1667 (1970).
[9] P. D. Maker, R. W. Terhune, M. Nisenoff, and M. Savage, Phys. Rev. Lett. **8**, 21 (1962).
[10] W. N. Herman and L. M. Hayden, J. Opt. Soc. Am. B **12**, 416 (1995).
[11] K. Wynne and J. J. Carey, Opt. Commun. **256**, 400 (2005).
[12] J. E. Bjorkholm, Phys. Rev. **142**, 126 (1966).
[13] T. K. Gustafson, J.-P. E. Taran, P. L. Kelly, and R. Y. Chiao, Opt. Commun. **2**, 17 (1970).
[14] T. K. Gustafson, J.-P. E. Taran, H. A. Haus, J. R. Lifsitz, and P. L. Kelly, Phys. Rev. **177**, 306 (1969).
[15] Y. J. Ding, Opt. Lett. **29**, 2650 (2004).
[16] A. Schneider, M. Neis, M. Stillhart, B. Ruiz, R. U. A. Khan, and P. Günter, J. Opt. Soc. Am. B **23**, 1822 (2006).
[17] F. Zernike, Jr. and P. R. Berman, Phys. Rev. Lett. **15**, 999 (1965).
[18] J. Morris and Y. R. Shen, Opt. Commun. **3**, 81 (1971); K. H. Yang, P. L. Richards, and Y. R. Shen, Appl. Phys. Lett. **19**, 320 (1971).
[19] L. Xu, X.-C. Zhang, and D. H. Auston, Appl. Phys. Lett. **61**, 1784 (1992).
[20] G. A. Askaryan, Sov. Phys. JETP **15**, 943 (1962).
[21] I. E. Tamm, *Sobranie Nauchnych Trudov* (Nauka, Moscow, 1975), Vol. 1, p. 77; J. Phys. (USSR) **1**, 439 (1939).
[22] G. M. Afanasiev, V. G. Kartavenko, and J. Ruzicka, J. Phys. A **33**, 7585 (2000).
[23] I. M. Frank and V. L. Ginzburg, J. Phys. (Moscow) **9**, 353 (1945).
[24] V. L. Ginzburg, Usp. Fiz. Nauk **172**, 373 (2002).
[25] V. L. Ginzburg and V. N. Tsytovich, *Transition Radiation and Transition Scattering*, The Adam Hilger Series on Plasma Physics (Hilger, Bristol, 1990).
[26] B. M. Bolotovskii, Proc. (Tr.) P.N. Lebedev Phys. Inst. **140**, 95 (1982).
[27] P. A. Cherenkov, Dokl. Akad. Nauk SSSR **2**, 451 (1934); S. Vavilov, *ibid.* **2**, 457 (1934).
[28] I. M. Frank and I. E. Tamm, Dokl. Akad. Nauk SSSR **14**, 109 (1937).
[29] U. A. Abdullin, G. A. Lyakhov, O. V. Rudenko, and A. S. Chirkin, Zh. Eksp. Teor. Fiz. **66**, 1295 (1974) [Sov. Phys. JETP **39**, 633 (1974)].
[30] D. H. Auston, Appl. Phys. Lett. **43**, 713 (1983); D. A. Kleinman and D. H. Auston, IEEE J. Quantum Electron. **QE-20**, 964 (1984).
[31] D. H. Auston, K. P. Cheung, J. A. Valdmanis, and D. A. Kleinman, Phys. Rev. Lett. **53**, 1555 (1984).
[32] D. H. Auston and M. C. Nuss, IEEE J. Quantum Electron. **24**, 184 (1988).

[33] J. K. Wahlstrand and R. Merlin, Phys. Rev. B **68**, 054301 (2003); S. K. Wahlstrand, T. E. Stevens, J. Kuhl, and R. Merlin, Physica B **316-317**, 55 (2002); T. E. Stevens, J. K. Wahlstrand, J. Kuhl, and R. Merlin, Science **291**, 627 (2001).

[34] M. Theuer, G. Torosyan, C. Rau, R. Beigang, K. Maki, C. Otani, and K. Kawase, Appl. Phys. Lett. **88**, 071122 (2006).

[35] M. Wang, O. Wada, and R. Koga, Appl. Opt. **35**, 3459 (1996).

[36] F. G. Bass and V. M. Yakovenko, Usp. Fiz. Nauk **86**, 189 (1965) [Sov. Phys. Usp. **8**, 420 (1965)].

[37] U. Happek, A. J. Sievers, and E. B. Blum, Phys. Rev. Lett. **67**, 2962 (1991).

[38] W. P. Leemans, C. G. R. Geddes, J. Faure, C. Toth, J. van Tilborg, C. B. Schroeder, E. Esarey, G. Fubiani, D. Auerbach, B. Marcelis, M. A. Carnahan, R. A. Kaindl, J. Byrd, and M. C. Martin, Phys. Rev. Lett. **91**, 074802 (2003); C. B. Schroeder, E. Esarey, J. van Tilborg, and W. P. Leemans, Phys. Rev. E **69**, 016501 (2004).

[39] N. N. Zinov'ev, A. S. Nikoghosyan, and J. M. Chamberlain, Phys. Rev. Lett. **98**, 044801 (2007).

[40] L. D. Landau and E. M. Lifshitz, *The Classical Theory of Fields* (Nauka, Moscow, 1973).

[41] J. D. Jackson, *Classical Electrodynamics* (Wiley, New York, 1962).

[42] Equation (10) and the following theory do not take into account chirping and broadening of the pump and terahertz pulses during their propagation in the nonlinear medium.

[43] A. Sommerfeld, *Partial Differential Equations in Physics* (Academic, New York, 1949).

[44] P. M. Morse and H. Feschbachm, *Methods of Theoretical Physics* (McGraw-Hill, New York, 1953).

[45] A. D. Polyanin, *Handbook of Linear Partial Differential Equations for Engineers and Scientists* (Chapman and Hall, Landon/CRC, Boca Raton, FL, 2002).

[46] We point out that very often, e.g., Refs. 11, 15, and 16 another set of BC, $E|_{z=0}=0$ and $dE/dz|_{z=0}=0$, is used to solve the radiation problem in a slab. It is worthwhile to note that such a choice of BC is physically unreasonable as it causes serious artifacts such as zero backward emission from the slab, etc.

[47] M. Born and E. Wolf, *Principles of Optics* (Pergamon, New York, 1970).

[48] N. Bloembergen, *Nonlinear Optics: A Lecture Note* (Benjamin, New York, 1965).

[49] R. W. Boyd, *Nonlinear Optics* (Academic, New York, 2003).

[50] Y. R. Shen, *The Principles of Nonlinear Optics* (Wiley, New York, 2003).

[51] A. Yariv, *Quantum Electronics*, 3rd ed. (Wiley, New York, 2001).

[52] Q. Wu and X.-C. Zhang, IEEE J. Sel. Top. Quantum Electron. **2**, 693 (1996); Appl. Phys. Lett. **70**, 1784 (1997).

[53] H. J. Bakker, G. C. Cho, H. Kurz, Q. Wu, and X.-C. Zhang, J. Opt. Soc. Am. B **15**, 1795 (1998).

[54] G. Gallot and D. Grischkowsky, J. Opt. Soc. Am. B **16**, 1204 (1999).

[55] V. G. Dmitriev, G. G. Gurzadyan, and D. N. Nikogosyan, *Handbook of Nonlinear Optical Crystals* (Springer, Berlin, 1997).

[56] D. T. F. Marple, J. Appl. Phys. **35**, 539 (1964).

[57] A. S. Barker, Jr. and R. Loudon, Phys. Rev. **158**, 433 (1967).

[58] S. Kojima, H. Kitahara, S. Nishizawa, and M. Wada Takeda, Phys. Status Solidi C **1**, 2674 (2004).

[59] B. E. A. Saleh and M. C. Teich, *Fundamentals of Photonics* (Wiley, New York, 1991).

[60] P. L. Kelly, IEEE J. Sel. Top. Quantum Electron. **6**, 1259 (2000).

[61] S. A. Akhmanov, V. A. Vysloukh, and A. S. Chirkin, *Optics of Femtosecond Laser Pulses* (AIP, Melville, NY, 1992).

[62] W. Shi, Y. J. Ding, N. Fernelius, and K. Vodopyanov, Opt. Lett. **27**, 1454 (2002).

[63] N. van der Valk, P. C. M. Planken, A. Buijserd, and H. Bakker, J. Opt. Soc. Am. B **22**, 1714 (2005).